

## Accepted Manuscript

Structural Design and Manufacturing Process of a Low Scale Bio-Inspired Wind Turbine Blades

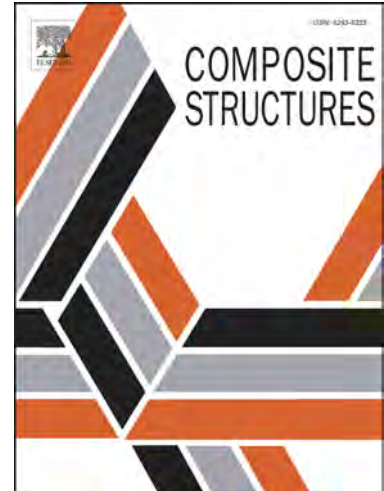
Camilo Herrera, Mariana Correa, Valentina Villada, Juan D. Vanegas, Juan G. García, César Nieto-Londoño, Julián Sierra-Pérez

PII: S0263-8223(18)30246-0

DOI: <https://doi.org/10.1016/j.compstruct.2018.08.061>

Reference: COST 10111

To appear in: *Composite Structures*



Please cite this article as: Herrera, C., Correa, M., Villada, V., Vanegas, J.D., García, J.G., Nieto-Londoño, C., Sierra-Pérez, J., Structural Design and Manufacturing Process of a Low Scale Bio-Inspired Wind Turbine Blades, *Composite Structures* (2018), doi: <https://doi.org/10.1016/j.compstruct.2018.08.061>

This is a PDF file of an unedited manuscript that has been accepted for publication. As a service to our customers we are providing this early version of the manuscript. The manuscript will undergo copyediting, typesetting, and review of the resulting proof before it is published in its final form. Please note that during the production process errors may be discovered which could affect the content, and all legal disclaimers that apply to the journal pertain.

# Structural Design and Manufacturing Process of a Low Scale Bio-Inspired Wind Turbine Blades

Camilo Herrera<sup>a,b</sup>, Mariana Correa<sup>a</sup>, Valentina Villada<sup>a</sup>, Juan D. Vanegas<sup>b</sup>, Juan G. García<sup>a</sup>, César Nieto-Londoño<sup>a,c</sup>, Julián Sierra-Pérez<sup>a</sup>

<sup>a</sup>*Grupo de Investigación en Ingeniería Aeroespacial, Universidad Pontificia Bolivariana, Circular 1 No. 73-34, Medellín, Colombia*

<sup>b</sup>*Grupo de Investigación en Nuevos Materiales, Universidad Pontificia Bolivariana, Circular 1 No. 73-76, Medellín, Colombia*

<sup>c</sup>*Grupo de Energía y Termodinámica, Universidad Pontificia Bolivariana, Circular 1 No. 73-34, Medellín, Colombia*

---

## Abstract

A wind turbine blade design inspired by a tree seed called *Triplaris Americana* is presented. The blade was designed by means of an analysis of the seed's curvature and airfoil along its wingspan; the result is as a non-conventional horizontal axis wind turbine composed of three blades. A computational fluid dynamic simulation was performed in order to estimate the operational loads. The blade's structure was designed by means of composite structural design, resulting in six zones with different laminates of carbon fiber. The balance of the aerodynamic and inertial loads was achieved in order to guarantee a minimum change in blade's geometry to prevent a performance reduction. Finally, a manufacturing simulation by means of vacuum assisted resin infusion was performed. Four injections strategies were proposed with three of them considered successful based on a complete mold filling and the time limit imposed by the polymerization time of the resin.

**Keywords:** Composites, Wind Turbine Blades, Aerodynamic Design, Vacuum Assisted Resin Infusion, Permeability

---

## 1. Introduction

Renewable energy has gained so much interest in the past few years, due to the necessity of generating eco-friendly electric energy making use of renewable resources like wind, solar, thermal and so on. Situations such as global warming and pollution have caused the improvement of wind energy harvested in order to generate electricity, avoiding the emission of polluting gases. Up to date, the wind energy market is more dominant than the solar technology market

in projects where big capacities are needed (dozens or hundreds of megawatts) [1], and despite of all the challenges to implement wind energy technology, the cost associated to all the stages (design, manufacture and operation) continues to reduce while a more standardized industry is growing up [2].

Although most of the work is concentrated in large scale wind turbines, in the last few years small and low scale wind speed turbines studies have been increased bit by bit with the purpose of such devices can be reachable to small industries and countries that can not afford wind farms with large ones or even do not have the appropriate wind conditions to operate them. So, aerodynamic and structural analyses are

---

*Email address:* julian.sierra@upb.edu.co (Julián Sierra-Pérez)

interesting topics to investigate due to the necessity of adapting both concepts in order to make the wind turbine more optimized to the operating conditions.

The research topic related to low scale wind turbines can be found into two categories: aerodynamics and structural analysis [3, 4, 5, 6, 7, 8] where it is necessary to adapt a correct and optimized shape in order to balance the aerodynamic loads with the structural ones in order to prevent deformations than can affect the performance of the blade itself.

Other important aspects include the wind resources as the basis of location that be able to provide not only enough wind with constant speed but also a good capacity to transmit the energy generated [8, 9, 10], and last but not least, the manufacturing process in which all the sketches are produced and assembled to form the wind turbine with the blades, the tower and the generator [7, 11, 12, 13].

Regarding to the blade itself, most of the times its design comes first due to its functionality to rotate in an axis to generate electric energy, so this is the start point of the wind turbine design and then, it can be developed the other main structures of the wind turbine such as the tower and the generation box [14]. With the application of wind turbines to supply the energy demand, these devices has become bigger and the materials choice is more complex, being composite materials the most used in the manufacturing process in order to support the extreme loads and stresses that turbines carry on [15]; as complement to this materials, it can be used honeycomb structures and foam core to optimize the stiffness and therefore the load distribution makes the structures more reliable to the loads.

The use of composite materials for wind turbines make the manufacturing process a little bit complex since so many variables are involved (viscosity, temperature, injection pressure, permeability, volumetric fiber ratio and the technique itself) [16, 17, 18, 19]. Such variables must be strictly controlled in order to obtain quality parts and a complete filling at the mold avoiding defects.

The inherent defects like voids or air bubbles that can appear in the part, should be minimized in order to manufacture high performance parts required in automotive and aeronautic-aerospace industries; ge-

nerally voids can appear due to the manufacturing process relative to the curing cycle, the injection strategies used or even by the nucleation of volatiles [20]. To overcome such problems it is often used computational simulations [21] in order to estimate the void formation and hence it can be possible to modify the manufacturing parameters before committing errors in the real part, so this led to a cost-effective process in order to avoid trial and error [22]. Finally, once all these issues be surpassed, the final part can be fabricated resulting in a less waste of material and money.

The objective of the current study is to present the structural design and manufacturing process of a very innovative wind turbine blades inspired on *Triplaris Americana* seed shape shown in Figure 1. The whole study starts from the design of a blade which preserves some of the aerodynamic characteristics of a seed belonging to a tree that grows in Colombia and another tropical regions of the Andes. The research includes several stages to develop, the aerodynamical one that is about the study of the blade and the wind turbine geometry in order to analyze the loads and the performance; the structural one in which a design of the stacking sequence of the composite plies was done to balance the blades inertial loads; then the manufacturing stage to study the resin infusion process was done by means of numerical simulations, to analyze the blade manufacturing behavior before real process and last but not least it was put in context the real performance of the wind turbine under various wind speeds.

It should be mentioned that exist other researches on the design of bio-inspired wind turbines like the single wind turbine blade inspired in maple seed [23], the three blade wind turbine also inspired on maple seed [24] and the wind turbine inspired by *Dryobalanops aromatica* seed [25].

## 2. Bio-inspired wind turbine blade design

### 2.1. Geometry

Early studies made by the current author García [26], established a blade shape (airfoil and curvature) bio-inspired by the *Triplaris Americana* seed, that

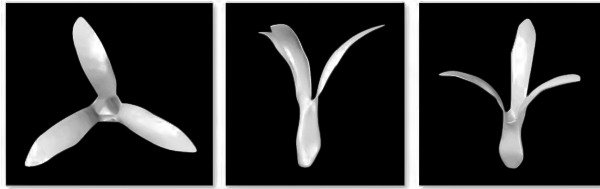


Figure 1: 3D model of *Triplaris Americana* seed.

has a particularly rotation movement when it falls off the tree. The seed grows in the Andes region, so it is very common to find in the flora of Colombia.

The authors performed two different studies: the first one consisted in the estimation of the seed's free fall speed and its corresponding angular speed; the second one consisted in the seed's airfoil and curvature characterization.

For the first part of the study, a 1.9 meters length and 40 cm diameter vertical wind tunnel was build for this purpose. More than 50 different seeds were used in this experiment. The results showed a mean free fall speed of 1.5 m/s with a related angular speed around 1500 RPM. The angular speed was measured by means of a laser tachometer.

For the second part of the study, the seed's airfoil was characterized from its cross section at different span points resulting in the average airfoil shown in Figure 2. More than 50 seeds (each one with three blades) were used in this study and for each blade, more than 10 traversal sections were studied. A similar process was performed in order to characterize the curvature of the seeds.

In a subsequent stage, both airfoil and curvature were used to perform an aerodynamic study in order to understand and unveil the aerodynamic behavior of the seed and be able to extrapolate such behavior to bigger geometries. The study was performed by means of computational fluid dynamics (CFD) considering a steady state and incompressible flow at low Reynolds number.

In order to validate the simulation method used in the aerodynamic study, a numerical validation was performed [4] by using the experimental data from NREL Phase IV wind turbine which has tested at NASA Ames Research Center [27] and comparing

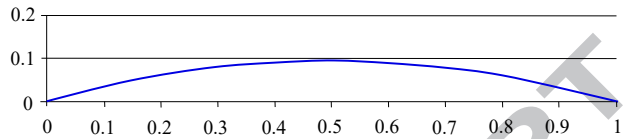


Figure 2: Seed average airfoil.

such data with CFD results. The NREL Phase IV wind turbine consist of two blades, but thanks to periodicity tools of CFD software it is enough to simulate only one blade and therefore a less computational cost is required.

The blade operation was simulated using the same CFD parameters used in the simulations performed to design the airfoil curvature in the previous step. Different wind speeds were simulated: 7 m/s, 10 m/s, 13 m/s, 15 m/s, 20 m/s, 25 m/s and the average error between the experimental data and the CFD results was 4.4%. This results show an excellent matching between experimental data reported and the CFD, so the simulation method is valid to perform an aerodynamic simulation of the bio-inspired wind turbine.

## 2.2. Geometry performance

After defining the airfoil and the curvature of the blades, a CFD simulation was performed with a 3D model of a three bladed wind turbine with the new blade design to calculate the torque, considering a diameter of 3.8 meters and a wind speed of 12.5 m/s, which is the nominal speed to produce the maximum power output. Then, the rotor power was calculated resulting in an output of 5.1 kW and hence the power coefficient ( $C_p$ ) performance was calculated within a speed regime from 3 m/s to 13 m/s as shown in Figure 3.

The main goal with the use of the *Triplaris* seed consisted in optimize the  $C_p$  at low wind speeds since the wind conditions in most Colombia and the Andean regions are very low, so producing energy from wind it is not efficient since there are not commercial turbines designed to operate at such conditions. The power curves were calculated (as seen in Figure 4) for different wind turbines diameters and for different wind speed; this graph is useful to estimate

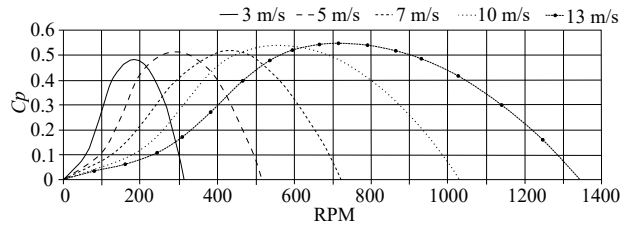


Figure 3:  $C_p$  performance at various wind conditions

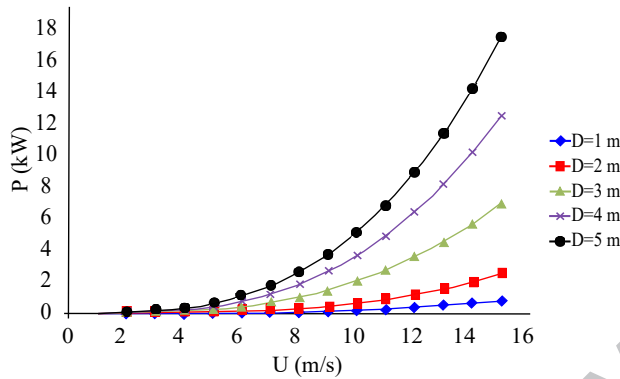


Figure 4: Power performance

the dimensions and operational conditions needed to meet a specific energy output.

### 2.3. Aerodynamic simulation

An aerodynamic simulation of the 3D model wind turbine shown in Figure 5 was performed. The patented design (PCT/IB2013/055783) was simulated at a wind speed of  $13 \text{ m/s}$  with an air density of  $1.225 \text{ kg/m}^3$  and a pressure of  $101325 \text{ Pa}$ ; additionally in order to preserve a balance between aerodynamic and inertial loads, the blade thickness was set variable increasing at the root section and reducing at the tip section. The main design criteria consisted in reduce the tip's deflection in order to not perturb so much the aerodynamic performance.

The results obtained showed an output power of  $5.1 \text{ kW}$ , besides, the pressure distribution along the blades was also calculated in order to determine the aerodynamic forces, since these values are an input parameter of the next simulation regarding to a fluid-structure interaction to develop a structural design



Figure 5: 3D model of Bio-inspired wind turbine.

that match the aerodynamic forces with the inertial ones, so the shape does not change and either its performance. In a previous research made by Correa et al. [4], more details about the aerodynamic design are presented.

### 2.4. Structural simulation

Before performing the structural simulation, the mechanical characterization of the materials involved in the wind turbine blades manufacturing was carried out. Two types of carbon fiber reinforced polymer (CFRP) were characterized [4]: unidirectional and a bidirectional fabric with 12K and 3K filaments respectively. Four different stacking sequences were used for the test specimens using layers oriented at  $0^\circ$ ,  $90^\circ$ ,  $45^\circ$  and  $-45^\circ$ . Specimens were manufactured by means of vacuum bag technique resulting in a fiber volume fractions of 57% and 49% for unidirectional and woven respectively.

The aim of the mechanical characterization was to obtain several mechanical properties in order to set them later as an input parameter of the fluid-structure interaction (FSI) simulation. The mechanical properties characterized for both reinforcements were: Young modulus ( $E_1$ ,  $E_2$ ), shear plane modulus

( $G_{12}$ ), Poisson ratio ( $\nu_{12}$ ), ultimate tensile strength ( $\sigma_u$ ), ultimate shear plain strength ( $\tau_u$ ), ultimate tensile strain ( $\varepsilon_{u1}$ ,  $\varepsilon_{u2}$ ), ultimate shear plane strain ( $\gamma_u$ ), mixed mode I/II ( $G$ ), interlaminar fracture toughness in mode I ( $G_{IC}$ ) and interlaminar fracture toughness in mode II ( $G_{IIC}$ ). All testing was performed under ASTM standards. Other thermal properties such as the coefficient of thermal expansion and the coefficient of moisture expansion were reported by the reinforcement manufacturer and were not characterized.

The obtained mechanical properties are presented in Table 1 and Table 2.

Table 1: CFRP properties.

Property	Unidirectional	Bidirectional
$E_1$ [GPa]	89.38	54.28
$E_2$ [GPa]	6.05	53.65
$G_{12}$ [GPa]	5.03	5.19
$\nu_{12}$	0.35	0.05
$\sigma_{u1}$ [MPa]	584.20	439.10
$\sigma_{u2}$ [MPa]	17.90	529.60
$\tau_{u12}$ [MPa]	31.90	51.48
$\varepsilon_{u1}$ [ $\mu\varepsilon$ ]	6500	8100
$\varepsilon_{u2}$ [ $\mu\varepsilon$ ]	3000	9900
$\gamma_{u12}$ [ $\mu\varepsilon$ ]	6300	9900

Table 2: CFRP interlaminar fracture toughness.

Property	DCB	MMB
$G$ [ $J/m^2$ ]	-	916.40
$G_{IC}$ [ $J/m^2$ ]	366	650.40
$G_{IIC}$ [ $J/m^2$ ]	-	236.20

For the interlaminar fracture toughness properties, two types of samples were used: DCB or Double Cantiliver Beam and MMB or Mixed Mode Bending.

With the mechanical properties of composite carbon fiber reinforcements and the wind turbine aerodynamic loads, the FSI simulation was carried out. The ANSYS module used is the Static Structural one [28]. In the ACP is defined the material, its mechanical properties, the stacking sequence and the fiber orientation of each ply.

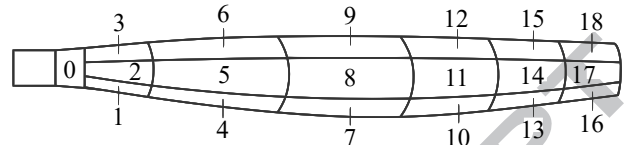


Figure 6: Blade zones.

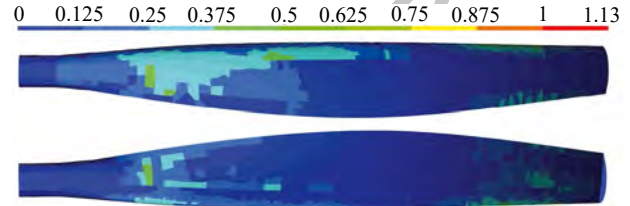


Figure 7: Maximum strain failure of extrados (top) and intrados (bottom) surfaces.

In an iterative way, the simulation estimates the strain distribution along the blade that has a set limits defined by a design criteria such as strains lower than 3000 microstrains and the blade tip displacement lower than 5 centimeters; additionally, maximum stresses are set regarding to the previously carbon fiber characterization. The final blade thickness is not constant because various zones experience more stress that led greater strains, thus, in order to optimize the material distribution and ensuring the blade will carry the loads, the blade was split into several areas (See Figure 6) taking into account the maximum strain failure distribution as shown in Figure 7. This distribution was obtained from the maximum strain criteria [29] and thanks to the Inverse Reverse Factor (IRF) a limit of one was set to determine if there is failure or not. Thus the contours of Figure 7 shows that none part exceed a value of 0.75.

The stacking sequence consists in six groups of laminates formed by  $0^\circ$ ,  $90^\circ$  and  $\pm 45^\circ$  carbon fiber plies. Such stacking sequences are listed in Table 3.

The laminates were considered balanced and symmetrical at the inner and outer blade surfaces, in other words, all six stacking groups are the same for the extrados and intrados surfaces. The blade itself weighs 3.8 kg that match perfectly with the low weight restriction in order to reduce the wind turbine inertia.

Table 3: Wind turbine blade laminates.

Laminate	Stacking sequence	Zones affected
1	45 -45	0-18
2	45 -45	0-10, 12, 15
3	0 90	0-4, 6, 9
4	0 0 0 45 -45	0-3, 6, 9
5	0 0 0 45 -45	0-3, 6
6	45 -45	0, 3, 6

#### 2.4.1. Structural and thermal checks

At the previous subsection both the aerodynamic and inertial loads were balanced, but the inertial ones generate higher strains so it is not possible to eliminate unnecessary material in the zones demarcated in Figure 8. However weight reduction gets more critical since it must be guaranteed an acceptable displacement at the tip of the blade and a homogeneous strain distribution along the blade in order to avoid an overload condition.

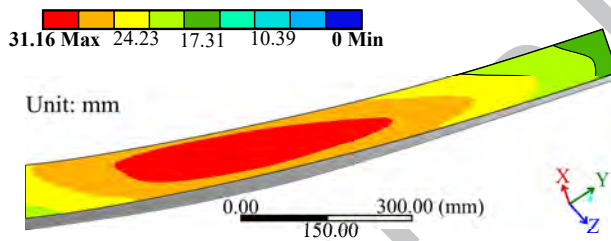


Figure 8: Total blade displacement at the tip.

Then a numerical simulation was started under nominal operation conditions with the stacking sequence obtained and the results show a total displacement of 31.1 mm at the tip section which meet the 50 mm requirement. This limit was imposed since from that value, the aerodynamic performance is not guaranteed due the blade deformation is too big.

As an overall view of total blade displacement shown in Figure 9, it can be seen that the higher displacement values are found in zones 13, 14 and 15 which are the most critical zones. The remaining ones do not show

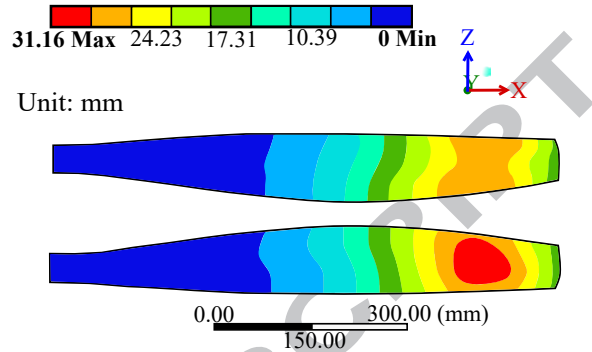


Figure 9: Total overall blade displacement.

important displacement that might affect the blade performance.

Additionally a safety factor (SF) was calculated based on the Colombian Institute of Technical Standards and Certification (IN-CONTEC) [30] taking into account the maximum strain level of 2157 microstrains, which it is localized at the leading edge or zone 15 where the aerodynamic loads predominate. The reference value to calculate de safety factor is the most critical one and it has 6300 microstrains as a result of the carbon fiber characterization under shear loads [4].

A safety factor of 2.92 was obtained. This value overcome the Colombian standards (IN-CONTEC) for metallic small wind turbines set in 1.35, and due to the complex mechanical behavior of this polymer matrix composites, the resulting reserve factor of 1.57 is considered appropriate for the design.

Since the whole blade is a monocoque structure composed by the intrados and the extrados, each one having symmetrical and balanced laminates and, at same time, being both symmetrical with respect to the mid plane of the airfoil, the mutual thermal coupling and the mutual influence coefficients (shear-extension, bending-extension and bending-twist) are counteracted. Therefore, no environmental warping or adverse coupling effects are expected as can be seen in Table 4.

Both thermal performance and mechanical performance were calculated before carrying out the numerical simulations by using ESA-COMP 4.6. The results were satisfactory and as mentioned before, no environmental warping nor undesirable mechanical warping was observed.

In order to perform the hygrothermal expansion validation, a reference environment defined by a temperature ( $T$ ) of 25 °C and a moisture weight percentage ( $w\%$ ) of 0.95 was defined. For this hygrothermal conditions the laminate is supposed to have the desired shape. Subsequently, a laminate load was defined based on a hot-wet environment ( $T = 50$  °C and  $w\% = 2$ ) and the resulting laminate expansion with the hygrothermal load was studied.

The thermal loads were considered as variable loads whilst the moisture loads were considered as constant loads. It is important to notice that external loads (aerodynamic and inertial loads) have an effect on the analysis even if they are supposed as zero. In this analysis, since the blade was designed in such way the aerodynamic loads counteract the inertial loads, the laminate expansion can be considered as unconstrained. Conversely, zero strains and curvatures mean constrained expansion.

As can be seen in the values reported in Table 4, the hygrothermal loads cause deformations of the mid plane laminates ( $\varepsilon_x^\circ$ ,  $\varepsilon_y^\circ$ ) with magnitudes below 355  $\mu\varepsilon$  for the  $x$  direction. On the other hand, as can be seen in Table 4, all the flexural strains in  $x$  direction are close to zero meaning that no warping effects occur.

From this study another variables were calculated such as the resultant expansion coefficients  $\alpha_x, \alpha_y$  and  $\alpha_{xy}$ ; the moisture expansion coefficients  $\beta_x, \beta_y$  and  $\beta_{xy}$  and the Kappa coefficients  $\kappa_x$  and  $\kappa_y$  that represent the curvature of the blade laminates. The combined strains are the sum of the constant part of moisture loads and the variable part of thermal loads. All the results are reported in Table 4.

The blade laminates that were defined in Ta-

ble 4 varies depending the zones defined in Figure 6. Thus, blade laminate 1 is composed by the overall sequence presented in Table 3, the second one eliminates the stacking sequence 6 (i.e. [45 -45]), the third one eliminates the stacking sequence 5 and so on until the blade laminate 6 is only composed by a fabric oriented at 45 degrees.

As mentioned before, external loads induce strains as well. Equivalent layer strains are the strains which induce actual layer stresses in a laminate. In a general case, the equivalent strains can be obtained by adding the residual strains and the strains due to external loads.

### 3. Manufacturing design

Once the design and material configuration were defined, the following step consisted in design an appropriate manufacturing technique which allows to obtain a quality blade with a cost-effective process.

Taking into account that this is the first blade design and it can be optimized in the future, and the blades are not going to be mass-produced yet, the mold might not be unique. Therefore a Vacuum Assisted Resin Infusion (VARI) technique was chosen to perform our research given that only uses one rigid mold so that results in a lower cost compared with other LCM techniques (i.e. Resin Transfer Molding RTM).

VARI is a process that offers high quality parts with low void formation or air entrapment thanks to the vacuum which is used, even in complex shapes such as wind turbine blades, it offers some advantages over the RTM process since the mold is submitted to less stress reducing the tooling cost, the volatile emission reduction due to closed mold technique, and also allows lower injection pressures [17, 31].

At this section the fluid and material characterization of two types of glass reinforcements (unidirectional and bidirectional) are presented. The experimental data obtained serves to validate a finite element simulation that allows to study several injection strategies for the wind turbine blade in order to choose the best one in terms of voids formation, injection time and complete mold filling.

Table 4: Resultant thermal expansion coefficients, moisture expansion coefficients, laminate flexural strains, mid-plane laminate strains and laminate curvatures.

Blade laminates	$\alpha_x$	$\alpha_y$	$\alpha_{xy}$	$\beta_x$	$\beta_y$	$\beta_{xy}$	$\hat{\varepsilon}_{fx}$	$\hat{\varepsilon}_{fy}$	$\varepsilon_x^\circ$	$\varepsilon_y^\circ$	$\kappa_x$	$\kappa_y$
	[ $10^{-6}/^\circ\text{C}$ ]			[ $10^{-2}/\text{w}\%$ ]			[ $\mu\varepsilon$ ]		[ $\mu\varepsilon$ ]		[ $1/m$ ]	
1	-0.115	7.79	0	0.011	0.0875	0	0	0	112.8	1113.3	0	0
2	-0.112	8.46	0	0.0111	0.0947	0	0	0	114.3	1205.8	0	0
3	0.15	6.55	0	0.0135	0.0749	0	0	0	145.0	950.2	0	0
4	2.03	2.03	0	0.029	0.029	0	0	0	355.6	355.6	0	0
5	1.97	1.97	0	0.0281	0.0281	0	0	0	344.4	344.4	0	0
6	1.85	1.85	0	0.0264	0.0264	0	0	0	323.9	323.9	0	0

It is important to clarify that the original design of the blade included carbon fiber/epoxy resin. However, at this part of the work the intention of the researches was to develop a design methodology of the manufacturing process based on finite element simulations which enables to extrapolate to any material setup. In this way, due costs and materials availability, it was decided to work with glass fiber/polyester resin for the experimental tests used later for the validation of the simulation methodology.

### 3.1. Permeability characterization

The permeability is perhaps, the main parameter to understand the flow behavior in the injection processes. The starting point is the commonly used Darcy's law that describes a flow through porous medium in order to analyze the flow rate and the pressure difference with a proportionality constant called permeability [32]. The flow behavior can be represented by Darcy's law vector form as follows [33, 34]:

$$\langle u \rangle = -\frac{K}{\mu} \nabla p, \quad (1)$$

where  $\langle u \rangle$  is the superficial speed,  $K$  the permeability tensor,  $\nabla p$  the pressure divergence and an associate fluid viscosity  $\mu$ . The superficial speed or Darcy flux is not the flow speed through the pores, but can be related with the porosity  $\phi$ :

$$v = \frac{u}{\phi}. \quad (2)$$

Assuming fabric reference axis coincides with Cartesian system axis and the pressure gradient has effects on the 3 directions, then the permeability is a tensor and it is represented in the following way:

$$K = \begin{bmatrix} K_x & 0 & 0 \\ 0 & K_y & 0 \\ 0 & 0 & K_z \end{bmatrix}.$$

This tensor is used when the reinforcement is considered anisotropic and generally, there are only used two directions  $x$  and  $y$ . In some cases like fabric reinforcements, the permeability in both axis can be considered equal so only one value needs to be calculated.

This model applies to a flow with the following properties [34, 35]: irrotational fluid, incompressible, low Reynolds Number ( $Re$ ) so inertial effects can be neglected, porosity keeps constant, gravitational effects can be neglected.

In order to calculate the permeability under Darcy's law, six tests were conducted with Permlab machine which it has a RTM mold with a transparent upper mold in order to capture the fluid flow and then calculate the permeability (See Figure 10). Two reinforcements were used, bidirectional glass fiber of  $180 \text{ gr}/m^2$  and unidirectional glass fiber of  $1030 \text{ gr}/m^2$ , for the first one, two tests were performed assuming  $K_1 = K_2$  due the fabric nature, on the other hand, for the unidirectional reinforcement four tests were performed each one with two repetitions for each fiber orientation ( $0^\circ$  and  $90^\circ$ ) because  $K_1 \neq K_2$ .

Due to the machine limitations, it was not used a

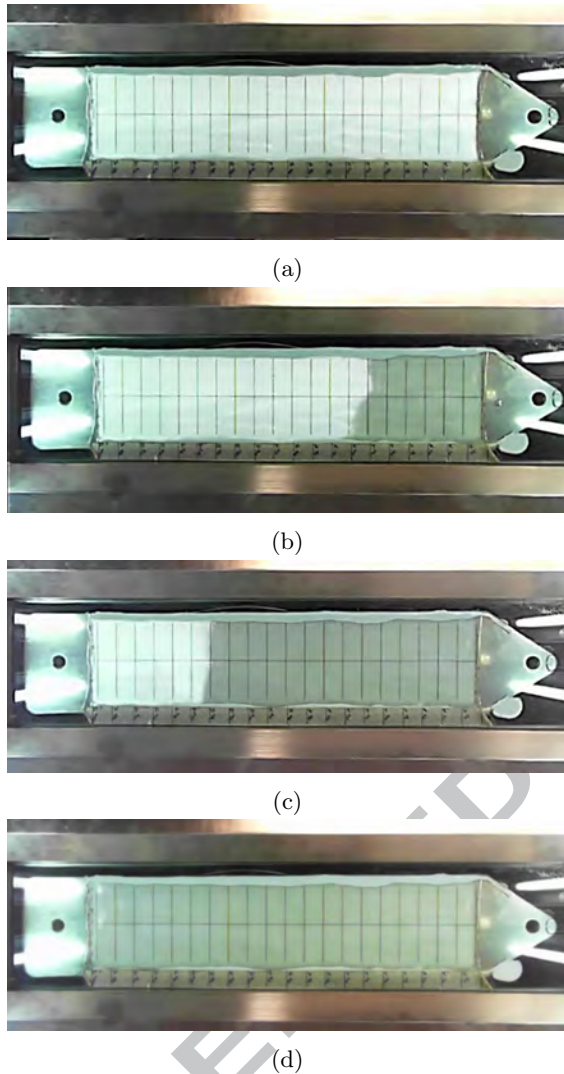


Figure 10: Filling sequence in Permlab mold. (a) 0%, (b) 30%, (c) 70%, (d) 100%.

polymeric resin in the characterization due its chemical properties and the tendency to damage some components, therefore a suitable substitute fluid was considered for experimentation that can reproduce the resin rheological behavior; most common replacement fluids are silicon oil, glycerin and vegetable oils [36] which have low viscosities and make them appropriate for RTM processes. After studying the

viscosity change respect to temperature, the results showed that silicone oil and vegetable oil has similar properties and it was chosen the vegetable oil as resin substitute fluid to be injected into the mold.

In the injection process there is an important effect that needs to be taken into consideration, this is the “racetracking”, this effect occurs when the fabric imperfections over the edges, generates a high permeability region and therefore the fluid flows faster affecting the calculations; generally this is caused by fabric damage during cutting process or even by an incorrect assembly [37]. In the rectangular Permlab mold the parallel sides to the flow direction can affect the permeability measurements due racetracking.

Hence, several tests were made in order to minimize this issue and thus not affect the permeability, the best six tests were taken into account for the calculations. An example of racetracking is shown in Figure 11, where part of the fluid flow found in the left side of flow direction is ahead of the main flow.

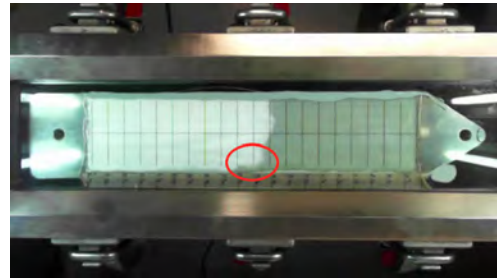


Figure 11: Racetracking.

The rest results are shown in Table 5, where three different values were calculated using Darcy’s law, one for bidirectional fabric and the remaining two for unidirectional reinforcement with permeability along the fibers and transverse permeability relative to the fiber orientation. In the calculus were not consider capillary effects because of this saturated method does not has influence in the final value [19].

The obtained permeability values were used as an input parameter of a finite element fluid flow simulations to understand the flow behavior on the wind turbine blade shape.

Table 5: Permeability values for bidirectional and unidirectional reinforcements.

Reinforcement	Fiber volume fraction (%)	Measured permeability (m <sup>2</sup> )	Average permeability (m <sup>2</sup> )
Bidirectional fabric	35.74	$8.86299e10^{-9}$	$7.24377e10^{-9}$
		$5.62455e10^{-9}$	
Unidirectional fabric. 0° orientation	62.02	$3.70564e10^{-9}$	$4.26457e10^{-9}$
		$4.82351e10^{-9}$	
Unidirectional fabric. 90° orientation	62.02	$2.75045e10^{-9}$	$3.11039e10^{-9}$
		$3.47032e10^{-9}$	

### 3.2. Numerical validation

To simulate the resin filling, it was used PAM-RTM software to understand the behavior of resin flow in the blade complex shape before the real manufacturing in order to avoid errors that would leave a poor quality blade. Before simulating the resin filling the blade's mold, it was done a validation of the model used with the help of radial injection tests in order to compare both flows for obtaining more accurate simulations. The radial mold consisted in a 40 cm x 45 cm cavity with a central injection point, so the fluid behaves in a divergent way; because of the fluid behavior, it was necessary to cut a circular hole at the center in order to avoid the fiber wash phenomena which consists in fiber displacement during the injection time [38], such phenomena can invalidate the complete test.

#### 3.2.1. Mesh study

Regardless the kind of mesh generator used, PAM-RTM restricts the mesh to triangular and tetragonal elements due the solving method for Darcy's law uses non-conforming elements [39]. Thus, with the purpose of create an adequate mesh, a convergence study was performed. This study allowed to know the minimum required number of mesh elements. This was done based on Wang et al. study [40] about numerical and experimental analysis of resin infusion, where it was analyzed the evolution of filling time versus the number of mesh elements until the filling time presented a steady behavior.

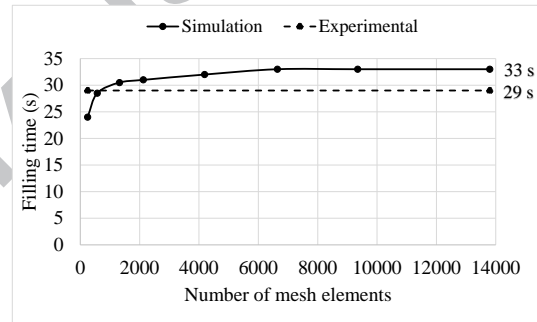


Figure 12: Filling time evolution vs. number of mesh elements.

A mesh with triangular elements was obtained from Patran mesh generator and as it is shown in Figure 12, the behavior is steady from 6000 elements where the filling time do not overcome 33 seconds. For the experimental tests the mean filling time was achieved at 30 seconds. The results were very similar to the numerical results.

Since the mesh was not too big and the computational requirements for the simulations are not high, the number of elements used for the numerical validation was 13500.

Later, various simulations were carried out for both bidirectional and unidirectional fabrics. The flow position was compared with the four semi-axis (radius) of the impregnated zone at a given filling time as it

is shown in Table 6 and Table 7.

There are differences between simulations and radial tests that can be accepted. The variability can be explained according to the following reasons [41]:

- Assembly errors because of perimeter bolts that tighten up the top mold; despite a torque wrench was used for close the mold.
- Flow front positions was calculated from the position of four semi-axis of saturated zone.
- It was not consider the top acrylic mold deformation. This material has a low elastic modulus of 6 GPa.
- Manipulation errors with reinforcement fabrics where cutting or positioning it in the mold. It could be affected the microscopically fiber tension causing deformations of fibers pattern. All of this could have done that the permeability varies affecting flow front and filling time.
- Permeability associated errors due to visual method for measuring flow front with a video.
- Capillary effects due to the nature of fiber reinforcement. The tests were performed at low injection pressure in order to eliminate flow front irregularities and to try that flow shapes as a circle, in case of bidirectional.
- Numerical error of simulation associated to the solution of the Darcy's equation.

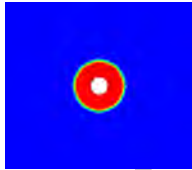
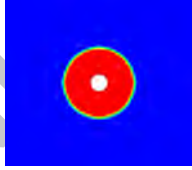
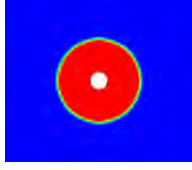
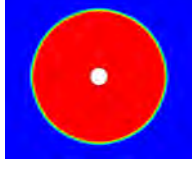
The comparison between numerical simulations and radial tests presented errors in their filling radius. To quantify the overall test error, in order to verify that there are not high excessive values, the relative error norm L2 was used. Such error can be expressed as follows:

$$e = \sqrt{\frac{\sum_{i=1}^{i=NOB} (u_s(i) - u_c(i))^2}{\sum_{i=1}^{i=NOB} u_s(i)^2}}, \quad (3)$$

where  $NOB$  is the number of data used to estimate the error,  $u_s$  is the exact solution value and  $u_c$  is the calculated value.

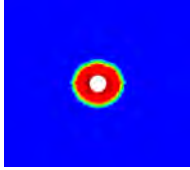
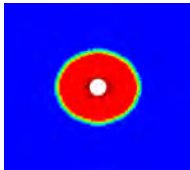
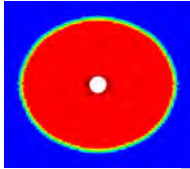
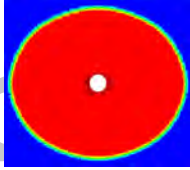
Data were taken from tests where  $u_s$  is the radial test value and  $u_c$  is the numerical simulation value. For the case of bidirectional reinforcement, the relative overall error estimated with equation 3

Table 6: Bidirectional fabric comparison.

Time (s)	Simulation ( $r = m$ )	Experimental ( $r = m$ )
1	0.0358 	0.034 
Difference: 5.29%		
2	0.0582 	0.053 
Difference: 9.81%		
3	0.0729 	0.065 
Difference: 12.15%		
9	0.1287 	0.12 
Difference: 7.25%		

was 8.63%, for unidirectional reinforcement in  $0^\circ$  fiber orientation the error was 14.2% and for  $90^\circ$  fiber orientation was 1.96%. The major difference was obtained for the  $0^\circ$  orientation, most probably due to the incorrect mold closure and the tighten of all the bolts despite the use of a torque wrench. In terms of distance, the maximum difference was 2.4 cm at the end of injection process, therefore the errors are not considered high given the mold size.

Table 7: Unidirectional fabric comparison.

Time (s)	Simulation ( $r = m$ )	Experimental ( $r = m$ )
1	$0^\circ = 0.0385$ , $90^\circ = 0.0316$ 	$0^\circ = 0.040$ , $90^\circ = 0.0325$ 
	Difference: $0^\circ = 3.75\%$ , $90^\circ = 2.77\%$	
3	$0^\circ = 0.073$ , $90^\circ = 0.060$ 	$0^\circ = 0.070$ , $90^\circ = 0.0585$ 
	Difference: $0^\circ = 4.29\%$ , $90^\circ = 2.56\%$	
15	$0^\circ = 0.156$ , $90^\circ = 0.132$ 	$0^\circ = 0.138$ , $90^\circ = 0.130$ 
	Difference: $0^\circ = 13.4\%$ , $90^\circ = 1.53\%$	
17	$0^\circ = 0.164$ , $90^\circ = 0.140$ 	$0^\circ = 0.140$ , $90^\circ = 0.143$ 
	Difference: $0^\circ = 17.14\%$ , $90^\circ = 7.69\%$	

### 3.3. Wind turbine blade simulations

After the reinforcement and resin experimental characterization and the numerical validation of the simulation method, the finite element model used in PAM-RTM was defined to study the filling process of the wind turbine blades under VARI molding techni-

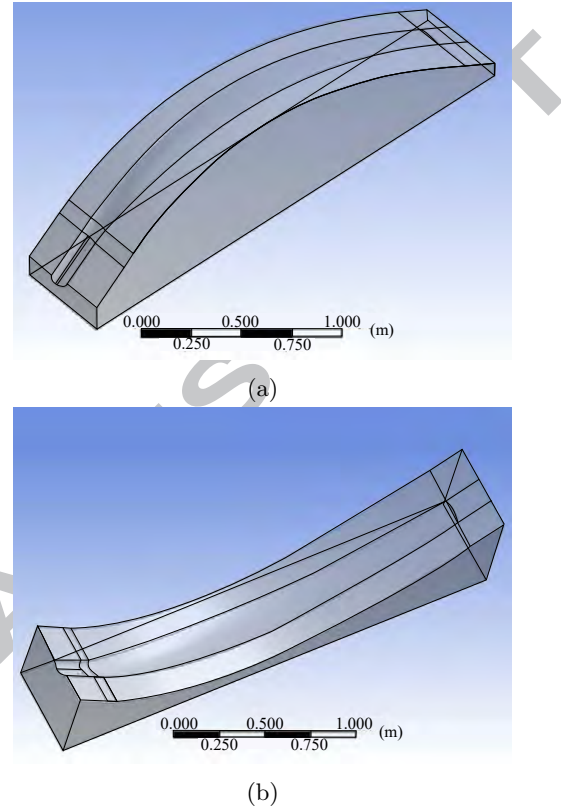


Figure 13: Wind turbine blade molds: (a) intrados and (b) extrados.

que. The parameters used in the simulations are: a polyester resin Altek R937-UPE-15 with a nominal viscosity of 150 cps and both reinforcements previously characterized with their permeability values from Table 5.

The blade geometry was split in two molds, one for intrados surface (See Figure 13a) and another for extrados surface (See Figure 13b). Then, both surfaces will be bonded together to form the blade. It is important to mention that the analysis was done to one blade separately, since the manufacturing process is the same for the remaining two.

The stacking sequences of the laminates were set in PAM-RTM from Table 3 taking into account the 18 zones in which the blade was divided previously, and due to symmetry the stacking sequences are the

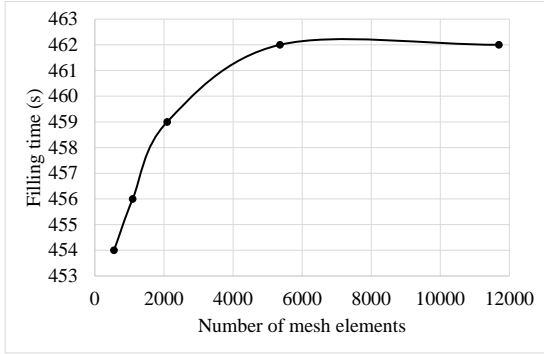


Figure 14: Extrados mesh study.

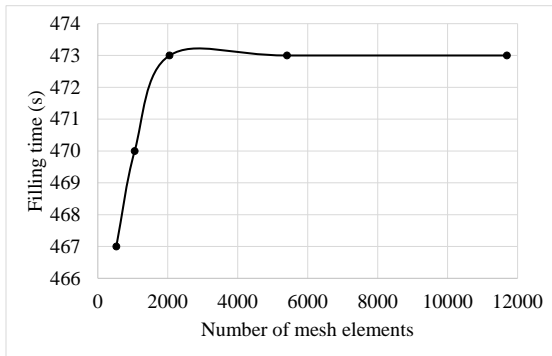


Figure 15: Intrados mesh study.

same for both extrados and intrados molds.

Similar to section 3.2.1, the same study was performed for the blade's mold (See Figures 14 and 15), analyzing the evolution of filling time versus the number of mesh elements. Because of there are two molds, the analysis was done separately for each one, resulting in a properly mesh with 6000 elements or above. This values are higher than the average, where time filling is steady since it was necessary to defined the 18 zones and a more refined mesh, besides this, a more accurate delimitation of each zone was necessary as well.

Once the permeability, viscosity, temperature, po-

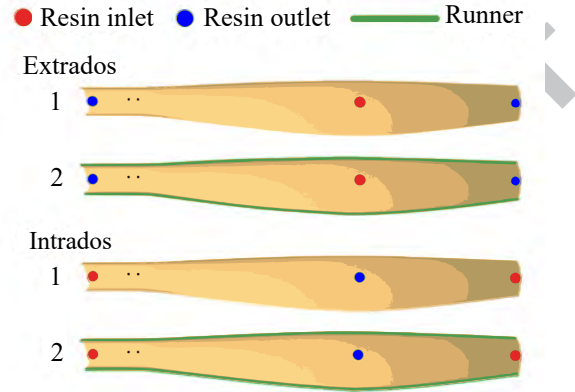


Figure 16: Injection strategies.

rosity, compressibility and pressure were set up in PAM-RTM, the next step consisted in define the injection strategies with the aim of getting the better options that can replicate the real injection completely well. Thus, four strategies were proposed considering the blade size and its complex shape, two for each concave and convex mold, since the gravity is relevant, the inlet and outlet ports must be different as it is shown in Figure 16.

Initially, six more strategies were studied from the research data published by Broad [13], however, the wind turbine blades he studied had a straight shape and the behavior of the resin filling the mold was completely different, therefore those strategies were not considered into the analysis presented in this research.

“Runners” were adding acting like channels with high permeability in order to force the resin to impregnate all the reinforcement. Thanks to previous simulations it was found that the blade mold edges tended to have a incomplete filling at the tip (See Figure 17) and the root, where the mold has sharp geometry.

Wind blade simulations implied that reinforcements architecture were not simple, these are a set of laminates as shown in Table 3, and located at different zones. Simulations were solved through a 2.5D mesh for both extrados and intrados molds in order

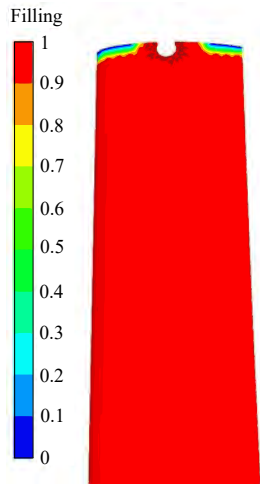


Figure 17: Incomplete tip filling for extrados.

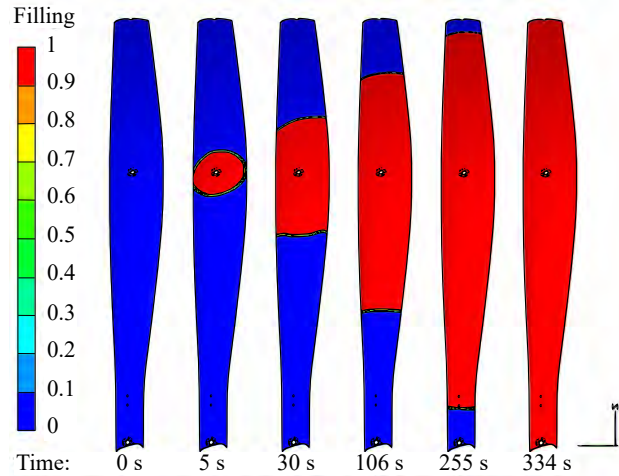


Figure 18: Flow front of strategy 1.

to capture the little effects at the tip and root edges, the mesh was defined in this way: 19280 triangular elements for extrados and 15592 for intrados. At this level the computational cost did not increased dramatically so the overall simulation time did not exceed 1 hour of computing time.

The simulation results are presented in Figures 18, 19, 20 y 21, they show the flow front evolution at different time lapses until the resin impregnates all the reinforcements. To define a complete and successful injection, two criteria were considered: the first one is based on resin gel time of 19.6 minutes (1176 seconds) with 1% in weight of catalyst, so the overall injection time has to be less than gel time. The second one is a complete resin impregnation, that means no air bubbles or voids can be present in the reinforcements over the whole injection process. From previous simulations, it was added runners over the edges and the center of the mold, however such strategy led to void formations for both molds so only the edge runners were taken into account.

In that terms, 1, 2 and 4 filling strategies were considered successful with filling times of 334, 184 and 296 seconds respectively, fulfilling the limit imposed by gel time. Besides, thanks to the runner, no voids were observed at the reinforcements, especially, at the critical points in the corners of the tip and the root

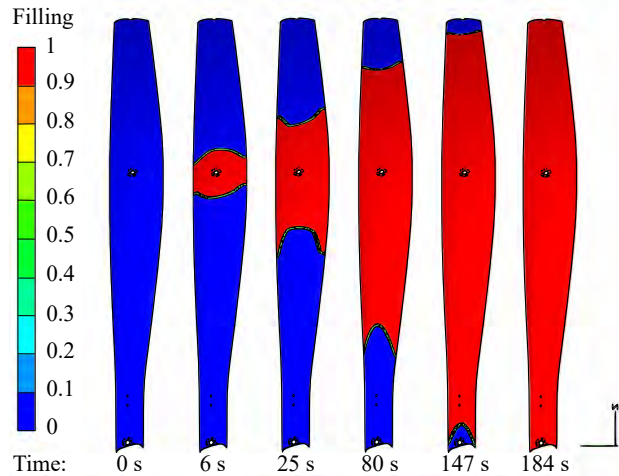


Figure 19: Flow front of strategy 2.

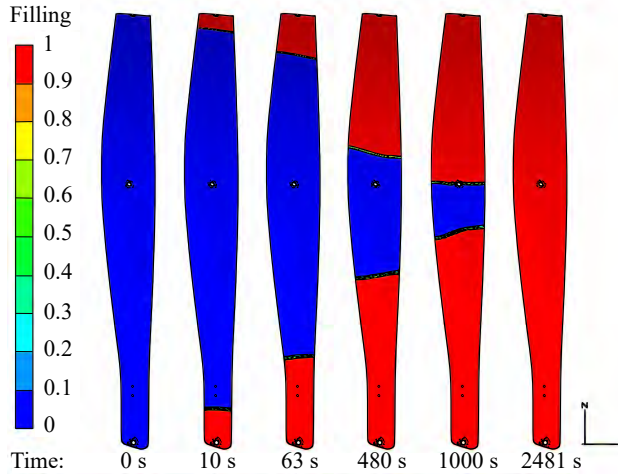


Figure 20: Flow front of strategy 3.

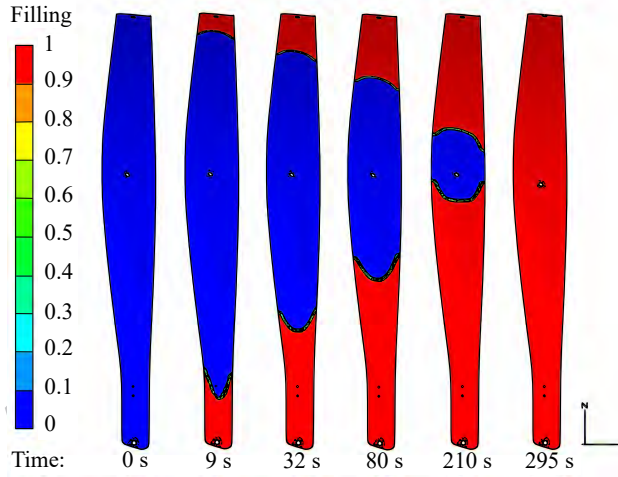


Figure 21: Flow front of strategy 4.

since the flow impregnated such areas first and then, continued to the resin outlet port.

The third strategy was not successful, mainly, due its filling time of 2481 seconds, exceeding the previous limit imposed; the bottom flow front presented a delay compared with the top flow front since the top flow reach the outlet port first and that affects the overall pressure at the mold making the flow run slower. Regarding the voids and air entrapment, the simulation did not show any defect in the whole filling because the software did not take the gel time limit; at real conditions the flow would stop near the 1196 seconds similar to the image associated to 1000 seconds (See Figure 20), leaving a big section of reinforcement dry.

#### 4. Wind turbine performance

A prototype of the wind turbine was manufactured in order to characterize the power conversion efficiency, since the worth of investment in this technology is based on the power coefficient improvement. The model has 3.8 meters in diameter and the blades are made of CFRP, preserving the stacking sequence analyzed in Table 3.

The wind turbine was mounted on a special designed device on a truck to be moved across a vast area with controlled quasi-stationary wind conditions (See Figure 22). The wind turbine protruded 6 meters over the truck in order to avoid undesirable interaction between them.

The tests were performed early in the morning when the natural wind speed was negligible and the wind speed interacting with the wind turbine was equal to the truck speed. Several runs were performed at different controlled speeds whilst the angular speed and the power of the wind turbine were acquired.

The power coefficient is shown in Figure 23. It can be seen that a minimum wind speed of 2.5  $m/s$  must be achieved to start producing energy. A peak in the  $C_p$  close to 0.55 was achieved during the tests, demonstrating a good energy conversion efficiency under real conditions.

Despite the fluctuating operational range, typical for wind turbines, the  $C_p$  is greater than other com-



Figure 22: Wind turbine test under real operational conditions

mercial examples compared with similar operational conditions and size. In the Table 8 [26], it was compared to the performance of the wind turbines and the results are pretty evident, the bio-inspired wind turbine has the greater value of  $C_p$  which means the energy conversion coefficient also has a greater value than the other examples presented.

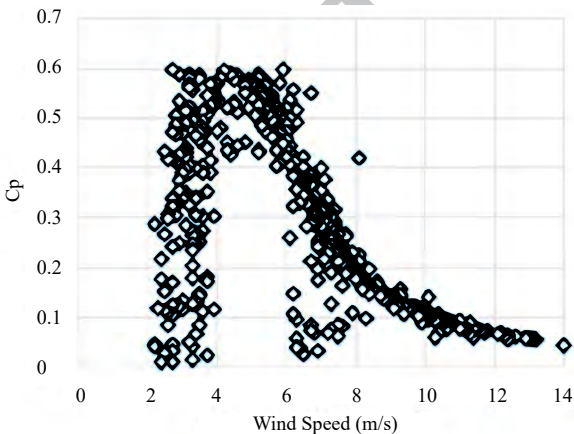


Figure 23: Experimental power coefficient

## 5. Conclusions

The aerodynamic design started from a previous study where a practical geometry was proposed to generate clean energy, where the wind turbine model was validated aerodynamically with errors below 8%. That allowed to obtain the pressure profiles to analyze the forces and torque to know the operational conditions of the wind turbine.

The mechanical properties of the reinforced gave the material limitations and therefore the strain distribution. There were proposed several zones with different laminates in order to withstand the forces induced by the operational loads and to obtain a maximum displacement of 31.1 mm at the blade's tip. In this way, the aerodynamic performance is not affected in a substantial way. Also, the stacking sequences were considered symmetrical and balanced to minimize coupling effects that could affect the blade shape.

For such a complex shape, it was necessary to perform a study to analyze the resin flow behavior involving all the stacking sequences and considering the permeability changes over the reinforcements, since any change in this parameter can lead to greater changes in the flow front. The permeability was characterized for two types of one single reinforcement ply and then the overall permeability of the laminates was approximate in the software considering the number of plies and the thickness.

The injection strategies gave an idea of how the resin will behave and the pressure and time requirements to complete a full impregnation. Several strategies were studied based on a straight blade shape, however, the results were unsatisfactory since gravity effect was neglected and the resin behavior break the limit imposed by time and filling, for this reasons those strategies were not included in this study. The strategies that were proposed considered a resin fluid front that flows against gravity in order to avoid additional accelerations that might leave air entrapment zones.

The use of runners helped the resin to reach zones that were difficult given the mold complexity, avoiding the formation of dry zones that are undesirable. Even this high permeability channels reduced

Table 8: Low scale wind turbines.

Manufacturer	Model	Power (kW)	Diameter (m)	speed (m/s)	$C_p$
Fortis	Passaat	1.4	3.1	16	0.0739
African Wind Power	AWP 3.8	2.0	3.8	12	0.0835
Windpower Enertec	Whisper 200	1	3	11.6	0.1480
Bergey	1500	1.5	3.2	12.5	0.1559
ACSA	LMW-1500	1	3.12	10.5	0.1845
Proven	Proven 2.5	2.5	3.5	12	0.2455
TechnoSpin	TSB 2000	2	3	12	0.2673
TechnoSpin	TSB 5000	5	3	14.5	0.3788
UPB	WINDSEED-01	5.1	3.8	12.5	>0.5

the overall filling time which implies that the pressure requirements can be reduced.

In general, the bio-inspired wind turbine performance overcome the various commercial wind turbines regarding to the power coefficient and hence the energy conversion factor. This particular geometry showed that the wind turbine has a great potential to generate electricity in areas where the wind speed is very low, being an excellent alternative for example, to developed countries that can not afford bigger and expensive devices.

### Future work

The results obtained suggest that the bio-inspired wind turbine has several limitations regarding to external parameters that can affect the performance like moisture and fatigue response, therefore it is necessary that a real model could be manufactured in order to analyze the structural behavior under real operational conditions. Also emulating the aerodynamic and generation response with severe weather, i.e. strong winds, rain, and the material degradation over time.

Another topic looking forward in the enhancement of the blade is the scaling to a bigger size to heavy electric generation. Two main paths can be traced, the study of the structural reliability and the analysis of the energy conversion as size and shape changes, if it is maintained or if it suffers some alteration.

### References

- [1] A. McCrone, U. Moslener, F. D'Estais, C. Grünig, Global Trends in Renewable Energy Investment 2017, 2017.
- [2] REN 21, Renewables 2017: global status report, 2017.
- [3] T. Bagherpoor, L. Xuemin, Structural Optimization Design of 2MW Composite Wind Turbine Blade, Energy Procedia 105 (2017) 1226–1233.
- [4] M. Correa-Álvarez, V. Villada-Quiceno, J. Sierra-Pérez, J. G. García-Navarro, C. Nieto-Londoño, Structural design of carbon/epoxy bio-inspired wind turbine blade using fluid/structure simulation, International Journal of Energy Research 40 (13) (2016) 1832–1845.
- [5] R. Barnes, E. Morozov, K. Shankar, Improved methodology for design of low wind speed specific wind turbine blades, Composite Structures 119 (2015) 677–684.
- [6] A. Albanesi, V. Fachinotti, I. Peralta, B. Storti, C. Gebhardt, Application of the inverse finite element method to design wind turbine blades, Composite Structures 161 (2017) 160–172.
- [7] G. Fernandez, H. Usabiaga, D. Vandepitte, Subcomponent development for sandwich composite wind turbine blade bonded joints analysis, Composite Structures 180 (2017) 41–62.

- [8] S. N. Akour, M. Al-Heydari, T. Ahmed, K. A. Khalil, Experimental and Theoretical Investigation of Micro Wind Turbine for Low Wind Speed Regions, *Renewable Energy* 116 (2017) 215–223.
- [9] U. Sangpanich, G. A. Ault, K. L. Lo, Economic feasibility of wind farm using low wind speed turbine, in: 2009 44th International Universities Power Engineering Conference (UPEC), 1–5, 2009.
- [10] B. H. Bailey, Wind resources for offshore wind farms: Characteristics and assessment, in: C. Ng, L. Ran (Eds.), *Offshore Wind Farms*, chap. 3, Woodhead Publishing, 29–58, 2016.
- [11] J. Yuan, C. Na, Y. Xu, C. Zhao, Wind turbine manufacturing in China: A review, *Renewable and Sustainable Energy Reviews* 51 (2015) 1235–1244.
- [12] U. E. Y. Gómez, Z. J. A. López, R. A. Jimenez, G. V. López, L. J. J. Villalon, Design and Manufacturing of Wind Turbine Blades of Low Capacity Using CAD/CAM Techniques and Composite Materials, *Energy Procedia* 57 (Supplement C) (2014) 682–690.
- [13] A. Broad, Development of Vacuum Assisted Composites Manufacturing Technology for Wind Turbine Blade Manufacture, Msc, University of Central Lancashire, 2013.
- [14] E. Hau, *Wind Turbines Fundamentals, Technologies, Application, Economics*, Springer-Verlag Berlin Heidelberg, 3 edn., 2013.
- [15] X. Lachenal, S. Daynes, P. M. Weaver, Review of morphing concepts and materials for wind turbine blade applications, *Wind Energy* 16 (2) (2013) 283–307.
- [16] S. Sharma, D. A. Siginer, Permeability Measurement Methods in Porous Media of Fiber Reinforced Composites, *Applied Mechanics Reviews* 63 (2) (2010) 1–19.
- [17] S. Bickerton, Q. Govignon, P. Kelly, Resin infusion/liquid composite moulding (LCM) of advanced fibre-reinforced polymer (FRP), in: *Woodhead Publishing Series in Civil and Structural Engineering*, chap. 7, 155–186, 2013.
- [18] N. K. Naik, M. Sirisha, A. Inani, Permeability characterization of polymer matrix composites by RTM / VARTM, *Progress in Aerospace Sciences* 65 (2014) 22–40.
- [19] D. S. Cairns, S. M. Rossell, Fluid Flow Modeling Of Resin Transfer Molding For Composite Material Wind Turbine Blade Structures, Tech. Rep., 2004.
- [20] J. Lambert, a.R. Chambers, I. Sinclair, S. M. Spearing, 3D damage characterisation and the role of voids in the fatigue of wind turbine blade materials, *Composites Science and Technology* 72 (2) (2012) 337–343.
- [21] S. Mouton, D. Teissandier, P. Sébastien, J. P. Nadeau, Manufacturing requirements in design: The RTM process in aeronautics, *Composites Part A: Applied Science and Manufacturing* 41 (1) (2010) 125–130.
- [22] J. R. Sayre, Vacuum-Assisted Resin Transfer Molding (VARTM) Model Development, Verification, and Process Analysis, Phd, Virginia Polytechnic Institute and State University, 2000.
- [23] S. Walters, H. A. Hegna, A Unique Single Blade Wind Turbine Senior Design Project, Joint Indiana-Illinois and North Central Sections of ASEE .
- [24] C. Seidel, S. Jayaram, L. Kunkel, A. Mackowski, Structural Analysis of Biologically Inspired Small Wind Turbine Blades, *International Journal of Mechanical and Materials Engineering* 12 (1) (2017) 19.
- [25] Y.-J. Chu, W.-T. Chong, A biomimetic wind turbine inspired by *Dryobalanops aromatica* seed: Numerical prediction of rigid rotor blade performance with OpenFOAM®, *Computers & Fluids* 159 (2017) 295–315.

- [26] J. G. García, Diseño aerodinámico de las palas de un aerogenerador inspiradas en semillas autorrotantes, Bsc, Universidad Pontificia Bolivariana, 2009.
- [27] M. Hand, D. Simms, L. Fingersh, J. Cotrell, S. Schreck, S. Larwood, Unsteady aerodynamics experiment phase VI: wind tunnel test configurations and available data campaigns, Tech. Rep., NREL: Golden, Colorado, USA, 2001.
- [28] ANSYS ®, Academic Research Static Structural, 2016.
- [29] L. S. Arias, L. Vanegas, Falla de los materiales compuestos laminados, *Scientia et Technica* (25) (2004) 113–118.
- [30] Instituto Colombiano de Normas Técnicas y Certificación INCONTEC, Aerogeneradores: Requisitos de diseño para aerogeneradores pequeños,, 2009.
- [31] C. Zhao, G. Zhang, Y. Wu, Resin flow behavior simulation of grooved foam sandwich composites with the vacuum assisted resin infusion (VARI) molding process, *Materials* 5 (7) (2012) 1285–1296.
- [32] D. Nield, A. Bejan, *Mechanics of Fluid Flow through a Porous Medium*, in: *Convection in Porous Media*, chap. 1, Springer-Verlag, New York, 1–26, 2013.
- [33] T. Lundström, R. Stenberg, R. Bergström, H. Partanen, P. Birkeland, In-plane permeability measurements: a nordic round-robin study, *Composites Part A: Applied Science and Manufacturing* 31 (1) (2000) 29–43.
- [34] A. George, *Optimization of Resin Infusion Processing for Composite Materials: Simulation and Characterization Strategies*, Phd, University of Stuttgart, 2011.
- [35] J. A. García, *Gestión del frente de avance en la modelización numérica del conformado por transferencia de resina (RTM)*, 2000.
- [36] J. D. Vanegas, *Análisis de propiedades físico-químicas de fluidos sustitutos para la medición de permeabilidad en procesos de inyección por molde cerrado*, Tech. Rep., Medellín, Colombia, 2011.
- [37] C. A. Vargas-Isaza, J. D. Vanegas-Jaramillo, I. D. Patiño-Arcila, *Methods for permeability measurements of fibrous reinforced preforms*, *Revista Facultad de Ingeniería Universidad de Antioquia* 72 (2014) 186–202.
- [38] S. Laurenzi, M. Marchetti, *Advanced Composite Materials by Resin Transfer Molding for Aerospace Applications*, in: N. Hu (Ed.), *Composites and Their Properties*, chap. 10, InTech, 197–226, 2012.
- [39] ESI Group, *PAM-RTM 2010 User's Guide & Tutorials*, 2010.
- [40] P. Wang, S. Drapier, J. Molimard, A. Vautrin, J. Minni, *Numerical and experimental analyses of resin infusion manufacturing processes of composite materials*, *Journal of Composite Materials* 46 (13) (2012) 1617–1631.
- [41] I. D. Patiño-Arcila, *Simulación por elementos de frontera del fenómeno de impregnación de preformas reforzantes empleadas en el proceso RTM*, Msc, Universidad Pontificia Bolivariana, 2013.